Leaky-Wave Sectorial Antennas for Passive 2-D DoA Applications

Leaky-Wave Sectorial Antennas for Passive Two-Dimensional DoA Applications

Matteo Perrone, *Student Member, IEEE*, Julien Sarrazin, *Senior Member, IEEE*, Guido Valerio, *Senior Member, IEEE*, Guido Lombardi, *Senior Member, IEEE*

***Abstract*—A fully metallic sectorial leaky-wave antenna (LWA) is proposed to perform passive two-dimensional direction-of-arrival (DoA) estimation. The LWA consists of a sectorial waveguide with periodic corrugations on the bottom plate and periodic slots on the top plate. The frequency dispersion of the waveguide is enhanced with a suitable choice of the geometric parameters of the corrugations using an analytical model. Two different corrugation shapes are selected: concentric and straight corrugations. The former one produces an isotropic dispersion, while the latter one produces an anisotropic dispersion of the aperture field when slots are etched to open the structure. In the open structure, the sectorial geometry and the circular slots allow for a 2D directional pattern in both azimuth and elevation, and straight corrugations lead to a stronger azimuth-dependent radiation pattern within the field of view. The performance of the LWAs for 2D DoA estimation are evaluated using the Multiple Signal Classification (MUSIC) algorithm. Results show that an anisotropic design of the corrugations enables a correct DoA estimation of both elevation and azimuth angles with a single-port antenna and with a fully passive system, being much more cost- and power-effective than traditional phased arrays.**

***Index Terms*—periodic structures, metasurfaces, leaky-wave antennas, direction-of-arrival estimation, MUSIC.**

I. Introduction

TWO-dimensional direction-of-arrival (DoA) estimation is essential in modern sensing and millimeter-wave (mmWave) communication systems, allowing precise spatial detection across both azimuth and elevation angles. Conventional solutions typically employ phased arrays, which offer beam-steering capabilities through active phase shifting across multiple elements. However, such systems are often bulky, expensive, and can lead to a high power consumption due to their reliance on active components [1]–[3].

Alternative solutions are offered by passive metasurfaces, cost-effective structures that enable the spatial modulation of phase and amplitude distributions in guided and radiated waves. They can be used to design leaky wave antennas (LWAs) [4]–[6] such as periodic slotted waveguides with corrugated plates [7]–[14], that enable controlled energy leakage within a desired frequency range allowing tailored frequency-beam scanning. This frequency diversity makes metasurface-based systems ideal for applications such as DoA estimation in complex scenarios. In this regard, the Multiple Signal Classification (MUSIC) algorithm [15], a widely used high-resolution technique, has proven to be effective for DoA estimation. Using the spatial covariance matrix of the received signals, MUSIC enables precise signal resolution in high-angular-resolution environments. However, LWA DoA two-dimensional estimation currently relies on multiport configurations [16], thus leading to complex front-end architectures.

M. Perrone and G. Lombardi are with Department of Electronics and Telecommunications (DET), Politecnico di Torino, 10129, Turin, Italy (email: matteo_perrone, guido.lombardi@polito.it).

J. Sarrazin and G. Valerio are with Sorbonne Université, CNRS, Laboratoire de Génie Electrique et Electronique de Paris, 75252, Paris, France and Université Paris-Saclay, CentraleSupélec, CNRS, Laboratoire de Génie Electrique et Electronique de Paris, 91192, Gif-sur-Yvette, France (email: julien.sarrazin, guido.valerio@sorbonne-universite.fr).

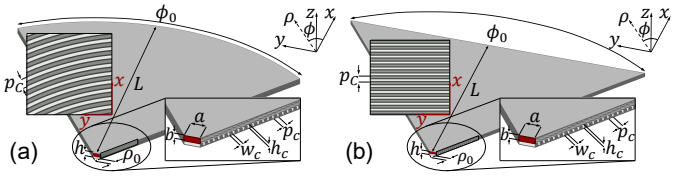

Fig. 1. Corrugated waveguides studied in this paper with the feeding in red. Sectorial waveguide (a) with concentric corrugations and, (b) with straight corrugations in the bottom plate. The geometric parameters are $\phi_0 = 73°$, $L = 210\,\text{mm}$, $\rho_0 = 4.8\,\text{mm}$, $a = 7.112\,\text{mm}$, $b = 2.556\,\text{mm}$, $h_c = 1.6\,\text{mm}$, $p_c = 2\,\text{mm}$, $w_c = 1\,\text{mm}$ ($h = b + h_c$).

This letter proposes a passive solution for DoA estimation using LWAs based on sectorial corrugated metasurface. The proposed LWA enables a two-dimensional and an azimuth-dependent directional pattern, scanning the elevation angle with frequency. By exploiting the azimuthal dependence of the frequency dispersion of the radiation pattern with appropriate signal processing, the DoA can be estimated over a 2D FoV using for the first time a single-port antenna, thus resolving with reduced complexity the azimuth ambiguity typical of conventional 2D-periodic LWAs [16]. This passive and low-cost novel structure is well suited for next-generation integrated systems where compactness and power efficiency are critical.

The paper is organized as follows. Section II describes the sectorial waveguides with corrugations on the bottom plate, and their dispersion properties. In Section III the LWAs are designed by etching concentric slots on the top plate and simulated results are presented. Section IV performs DoA estimation using the proposed LWAs with MUSIC algorithm. Conclusions are drawn in Section V.

II. Corrugated sectorial waveguides

We aim at designing a LWA with an enhanced frequency dispersion in the operating frequency range, having a directional pattern along two principal planes and exhibiting different scanning rates according to the azimuthal observation point. To achieve this goal, the underlying hypothesis in this work is that an azimuth-dependent frequency dispersion of the LWA beam direction can be achieved with a leaky waveguide exhibiting

different frequency dispersion along different propagation directions, i.e. a dispersion anisotropy (DA). In this section, we describe sectorial waveguides having the desired dispersion properties, while in the following one, we design the LWA by opening slots on the top of the closed structures.

The closed sectorial waveguides are shown in Fig. 1. They have an angular aperture ϕ_0, a radial length L, and are fed by a rectangular waveguide placed at a distance ρ_0 from the sector center. These waveguides are here completely shielded with top, bottom, and lateral PEC boundaries [17], [18]. The angular aperture $\phi_0 = 73°$ is chosen in order to cover a wide FoV (60° and 100° in azimuth as shown in Section IV), which requires small apertures, characterized by a noticeable effect of the DA, achievable with large apertures.

We use a cylindrical coordinate system (ρ, ϕ, z) centered in the sector center. The waveguides have a symmetry plane at $\phi = 0$. A TM^z polarized wave is excited in the waveguides, travelling along the $+\rho$ direction with a radial dependence represented by Hankel functions of the second kind and order q, $H_q^{(2)}(k_\rho\,\rho)$, and a sinusoidal azimuthal behavior to fulfill boundary conditions on side plates [18], [19]. $k_\rho = \beta - j\,\alpha$ is the radial wavenumber, where β and α are the radial phase and attenuation constants, respectively. The frequency dispersion of the structure (variation of β vs. frequency) is enhanced by inserting periodic corrugations in the bottom plate and suitably varying their height. The waveguide is assumed lossless, so $k_\rho = \beta$. As discussed in [9], we feed the structure with a rectangular wabeguide port which excites the fundamental TM_{01}^z propagating mode in the sectorial waveguides.

To increase the frequency dispersion of the waveguides (that is, to decrease the slope of the dispersion curve in a Brillouin diagram frequency vs. β), corrugations can be designed to exhibit a bandgap close to the operating frequency range. In our case, for mmWave sensing applications, the chosen range is $[26.5, 29.5]$ GHz. The increased frequency dispersion enables a faster frequency scanning in the LWA. By varying the corrugation height h_c, we evaluate the frequency dispersion of a parallel-plate waveguide having straight corrugations by using the analytical model for in [20], considering the wave propagation perpendicular to the corrugations. The analytical model in [20] is obtained with the assumption that the period p_c and the width w_c of the corrugations are much smaller than the operating wavelength [21]. Then, the period $p_c = 2\,\mathrm{mm}$, and width $w_c = 1\,\mathrm{mm}$ are chosen. Fig. 2a shows the dispersion diagrams obtained varying h_c. Increasing h_c makes the structure more dispersive, enabling faster frequency scanning. However, large h_c values bring to operating near the bandgap, increasing metallic losses and worsening input matching, which reduces antenna gain. Consequently, $h_c = 1.6\,\mathrm{mm}$ is chosen as a tradeoff between dispersion and efficiency. Two different corrugated bottom plates are designed: concentric corrugations in Fig. 1a and straight corrugations in Fig. 1b, both being symmetric with respect to $\phi = 0$. To analyze the dispersion using Ansys® HFSS software and the adjacent-zeros method (AZM) as discussed in [9], a travelling wave behavior is enforced by terminating both structures with absorbing boundary conditions and with the end contour of the same shape as the corrugations (i.e., circular end for Fig. 1a, straight end in Fig. 1b). Fig. 2b shows dispersion diagrams for $h_c = 1.6\,\mathrm{mm}$, $p_c = 2\,\mathrm{mm}$, and $w_c = 1\,\mathrm{mm}$. Results are computed with the analytical model and using the AZM for both structures and for two ϕ-directions, i.e., $\phi = 0$ and $\phi = 3\,\phi_0/8$ (in the middle and close to the lateral plate of the waveguides, respectively). Analytical model is in good agreement with $\phi = 0$ numerical results. For the sectorial waveguide with concentric corrugations (SWCC), we have a superposition of the curves along the two angles (light blue and green dashed curves). In the sectorial waveguide with straight corrugations (SWSC), we can observe instead different dispersions according to the angle of propagation (violet and dark blue dashed curves). This confirms the evident dispersion isotropy of SWCC and the DA of the SWSC.

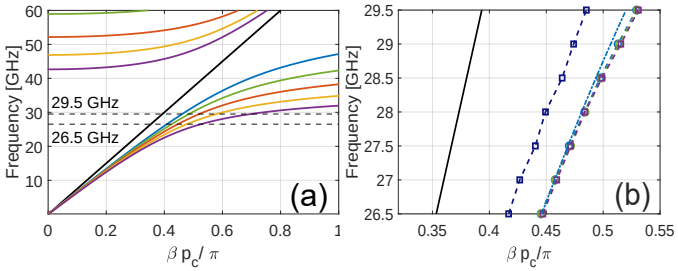

Fig. 2. Normalized (to $p_c = 2\,\mathrm{mm}$) dispersion diagrams. (a) Corrugated PPW for different corrugation height h_c using the analytical model [20]. $h_c = 2\,\mathrm{mm}$ (*violet*), $h_c = 1.8\,\mathrm{mm}$ (*yellow*), $h_c = 1.6\,\mathrm{mm}$ (*orange*), $h_c = 1.4\,\mathrm{mm}$ (*green*), $h_c = 1.2\,\mathrm{mm}$ (*light blue*) curves. (b) SWCC and SWSC at $\phi = 0, 3\,\phi_0/8$ with the AZM and, analytical model [20] for $h_c = 1.6\,\mathrm{mm}$. Light lines k_0 (*black lines*).

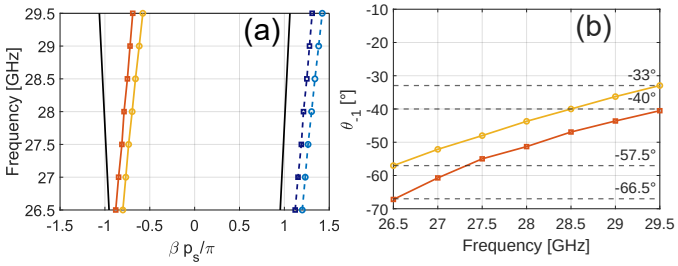

Fig. 3. (a) Normalized (to $p_s = 5.4\,\mathrm{mm}$) dispersion diagrams for the SWCC and SWSC, at different ϕ-directions, obtained by (1) and the results in Fig. 2b. Fundamental harmonic β of the SWCC along any ϕ directions and of the SWSC along $\phi = 0$ (*light blue dashed line*). Visible harmonic β_{-1} of the SWCC along any ϕ direction and of the SWSC along $\phi = 0$ (*yellow solid line*). Harmonics along $\phi = 3\phi_0/8$ of the SWSC: fundamental harmonic (*dark blue dashed line*) and visible harmonic (*orange solid line*). Light lines $\pm k_0$ (*black lines*). (b) Predicted elevation angles of the antennas, obtained from β_{-1} (1).

III. Sectorial Leaky-Wave Antennas

A. Dispersion design

As shown in Fig. 2b, in both corrugated waveguides the guided modes are in the slow-wave region for any ϕ values, i.e., $\beta > k_0$. In order to radiate, the approach chosen here is to etch on the top plate a series of concentric slots having the same (radial) width w_s and the same radial distance p_s between them. This creates a radial periodicity and produces higher-order harmonics whose phase constant is β_n, possibly radiating (if in the fast region $-k_0 \le \beta_n \le k_0$) at an elevation angle θ_n [4]:

$$\beta_n = \beta + 2n\pi/p_s, \qquad \theta_n = \sin^{-1}(\beta_n/k_0) \tag{1}$$

with $n = 0, \pm1, \pm2, \ldots$, where β is the radial phase constant of the fundamental harmonic, assuming the same as the phase constant of the guided modes in the closed structure. This is a common hypothesis and is confirmed by the following results of radiation properties.

Varying p_s, fast (visible) harmonics can be generated in the forward and backward ranges, i.e. $0 < \beta_n < k_0$ and $-k_0 < \beta_n < 0$, respectively. The value of p_s is chosen in order to obtain one visible harmonic in each structure with a pronounced frequency scanning. For a given frequency dependency of β and due to the nonlinear shape of the $\sin^{-1}$ function in (1), the frequency scanning is faster far from broadside than around broadside, where the behavior is approximately linear. For this reason, in order to stay far enough away from the broadside, the value $p_s = 5.4\,\text{mm}$ is chosen in both structures.

In Fig. 3a, the dispersion diagram of the fundamental harmonic (dashed lines) and the backward -1 visible harmonic (solid lines) obtained using (1) are shown. In particular, while the harmonics in the SWCC do not depend on ϕ, in the SWSC vary according to the ϕ propagation direction (results for $\phi = 0$ and $\phi = 3\,\phi_0/8$ are shown). Since the propagation along $\phi = 0$ is the same for SWCC and SWSC, we show only one curve in this case.

Following our hypothesis that the DA translates into an anisotropic behavior of the frequency dispersion of the LWA beam direction (θ_n), and further assuming that the θ_n for a given ϕ mainly depends on the phase constant experienced by the guided wave along that same ϕ, the θ_n is estimated using (1) and the backward -1 visible harmonics of Fig. 3a. Although the radiated pattern along each direction depends on the entire aperture field, it is shown later that this assumption is relevant when predicting the beam direction and its frequency variation. Fig. 3b shows that the SWSC exhibits not only different elevation beam directions, but also different frequency variation depending on ϕ ($\Delta\theta = 24.5°$ and $\Delta\theta = 26.5°$, for $\phi = 0$ and $\phi = 3\phi_0/8$, respectively).

B. Antenna design

The radiating properties of the sectorial LWAs with concentric corrugations (LWACC) and straight corrugations (LWASC) are discussed in this section. 38 slots are etched on the top plates, all with a radial width of $w_s = \lambda_0/5$, where λ_0 is the free-space wavelength at central frequency of 28 GHz. The geometries of the periodic LWAs are illustrated in Fig. 4.

A radial length $L = 210$ mm was chosen to radiate most of the power before the end of the antennas [4]. This was verified after checking that the structures were well matched in the considered bandwidth, as confirmed by the reflection coefficient $|S_{11}|$ of the LWAs in Fig. 4c, lower than $-15\,\text{dB}$ without the need for initial corrugation or slot tapering. The power reaching the end of the antennas was evaluated by defining a second waveguide port at the end of the LWASC and computing the transmitted power $|S_{21}|$ [22]–[24]. Due to the width of the second waveguide port, five modes were defined

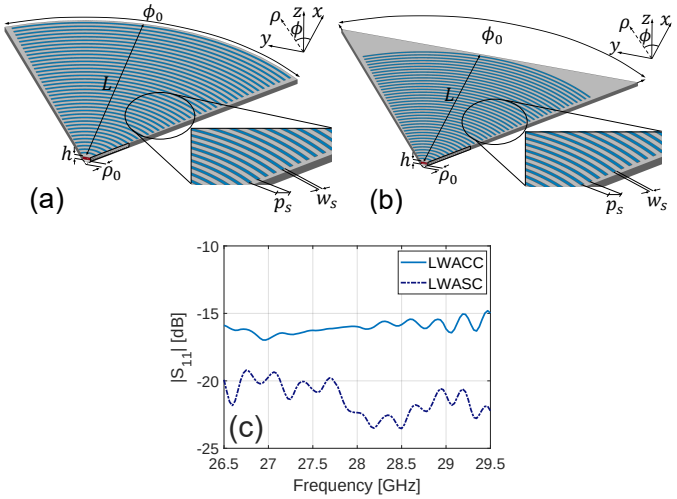

Fig. 4. Corrugated LWAs with feeding in red. Sectorial LWAs with concentric slots in the top plate and: (a) concentric corrugations, (b) straight corrugations in bottom plate. The geometric parameters are $\phi_0 = 73°$, $L = 210\,\text{mm}$, $\rho_0 = 4.8\,\text{mm}$, $p_s = 5.4\,\text{mm}$, $w_s = 2.14\,\text{mm}$. (c) $|S_{11}|$ of the LWAs.

on it, and five transmission coefficients were computed. The coefficient related to the first mode is lower than -10 dB in the considered frequency band, while the higher order modes were more strongly attenuated. This confirms that the chosen L is sufficient to radiate most of the power through the slots. The results are not shown here for brevity.

The 2D realized gain for the two LWAs is shown in Fig. 5 for the lower and upper frequencies of the considered bandwidth. To compare the gain with the beam directions predicted in Fig. 3b, the same ϕ directions, i.e., $\phi = 0$ and $\phi = 3\,\phi_0/8 \approx 27.5°$ are selected in Fig. 5. The corresponding θ of maxima of the gain are in good agreement with the θ_{-1} predicted in Fig. 3b for structures with concentric and with straight corrugations. The θ angular scanning within $[26.5, 29.5]\,\text{GHz}$ is $\Delta\theta = 27.5°$ for the LWACC (for any ϕ value) and for the LWASC for $\phi = 0°$, and $\Delta\theta = 30.5°$ for the LWASC for $\phi = \pm 27.5°$ (due to the symmetry of the structures at $\phi = 0$). This azimuthal dependence of the θ frequency-scanning rate is leveraged in the next section for simultaneous θ/ϕ DoA estimation.

IV. Direction-of-Arrival Estimation

A. MUSIC algorithm applied to LWA

The DoA estimation is performed here using the MUSIC algorithm that processes the covariance matrix of signals received by the LWA. The system model assumes D sources using a multicarrier modulation scheme, impinging on the LWA as $D\,(d = 1, ..., D)$ plane waves. Furthermore, considering only the subcarriers that are modulated by the same symbol [10], the received signal is expressed in the frequency domain as:

$$\mathbf{x}[k] = \mathbf{A}\mathbf{s}[k] + \mathbf{z}[k], \tag{2}$$

where $\mathbf{x} \in \mathbb{C}^{M\times1}$ is the received vector, M is the number of frequency samples, $k = 1, ..., K$ is the kth snapshot among K, $\mathbf{A} \in \mathbb{C}^{M\times D}$ is the LWA response matrix, $\mathbf{s} \in \mathbb{C}^{D\times1}$ is the source vector, representing the complex amplitudes of the D sources and $\mathbf{z} \in \mathbb{C}^{M\times1}$ is a complex additive white Gaussian

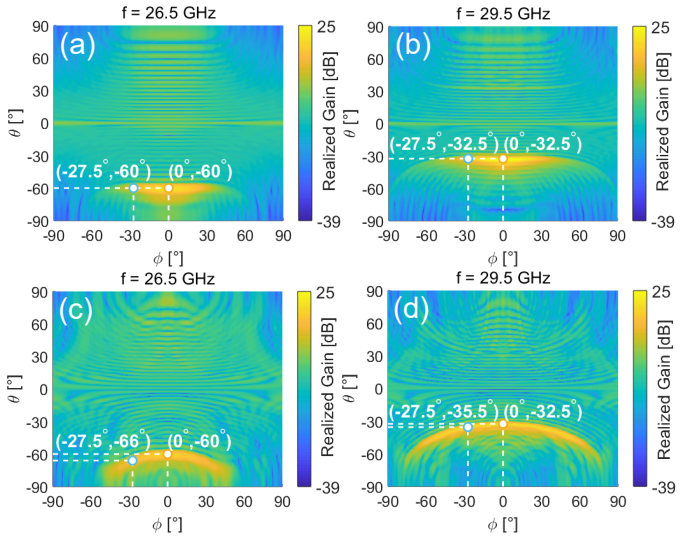

Fig. 5. Realized gain in the H-plane for two frequencies. (a) and (b) gain of the LWACC, (c) and (d) gain of the LWASC.

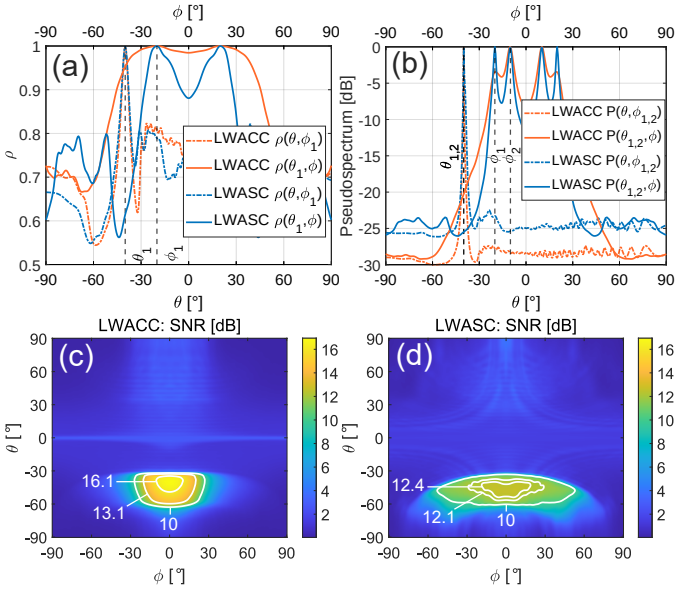

Fig. 6. (a) Autocorrelation ρ for one source at $\theta_1 = -40°$, $\phi_1 = -20°$, (b) pseudo-spectrum with 2 sources $\theta_{1,2} = -40°$, $\phi_1 = -20°, \phi_2 = -10°$ with $K = 25$, $M = 49$, with an SNR (c) for LWACC and (d) for LWASC.

noise (AWGN) vector with uncorrelated components. Each column of $\mathbf{A}$, i.e., $\mathbf{a}(\theta_d, \phi_d)$, is the LWA frequency response for an incident plane wave with (θ_d, ϕ_d) DoA and is obtained with HFSS simulations. It is important to note that M is the number of frequency samples, i.e. subcarriers, as opposed to the number of antenna elements in a traditional linear-array-based MUSIC scenario. To estimate the DoA, the covariance matrix is first estimated from the received signal as:

$$\hat{\mathbf{R}} = \frac{1}{K} \sum_{k=1}^{K} \mathbf{x}[k]\, \mathbf{x}^H[k], \tag{3}$$

where $(\cdot)^H$ denotes the Hermitian transpose. The null space of the covariance matrix is computed, and the MUSIC pseudospectrum is defined as:

$$P(\theta, \phi) = \frac{1}{\mathbf{a}^H(\theta_d, \phi_d)\mathbf{E}_N\mathbf{E}_N^H\mathbf{a}(\theta_d, \phi_d)}, \tag{4}$$

where $\mathbf{a}(\theta_d, \phi_d)$ is the steering vector for an incoming wave at angles (θ_d, ϕ_d), $\mathbf{E}_N$ is the noise subspace of the covariance matrix $\hat{\mathbf{R}}$. The peak in the pseudo-spectrum corresponds to the estimated DoAs of the incoming signals.

B. Results

The autocorrelation, defined as $\rho = |\mathbf{a}^H(\theta_d, \phi_d)\, \mathbf{a}(\theta_d + d\theta, \phi_d + d\phi)| / \|\mathbf{a}(\theta_d, \phi_d)\| \|\mathbf{a}(\theta_d + d\theta, \phi_d + d\phi)\|$, is shown in Fig. 6a for both LWASC and LWACC with one $d = 1$ source at $\theta_1 = -40°$, $\phi_1 = -20°$. The autocorrelation represents the gain frequency-variation similarity experienced between sources impinging at two different angles. It can be observed that both antennas exhibit a single $\rho = 1$ peak at the DoA location along θ. In the ϕ plane, the autocorrelation behavior is almost flat around ϕ_1 with the LWACC. This is due to the isotropic behavior of the LWACC pattern along ϕ and thus suggests weak $\hat{\phi}$ estimation performance. The LWASC, thanks to its anisotropic behavior, does exhibit a sharper peak at ϕ_1, which suggests improved $\hat{\phi}$ estimation performance. Both antennas exhibit a symmetric behavior in the ϕ plane, which leads to $\pm\hat{\phi}_1$ ambiguity. To assess the DoA estimation capabilities of the structures, the MUSIC pseudospectrum is shown in Fig. 6b, with the simulation parameters given in the caption. The scenario considers $d = 2$ sources with identical $\theta_{1,2} = -40°$ and different $\phi_1 = -20°$ and $\phi_2 = -10°$. For the LWA-based MUSIC, each source experiences an SNR $= \|\mathbf{a}(\theta_d, \phi_d)\|^2 \mathbb{E}\left[|s_d[k]|^2 / \|\mathbf{z}[k]\|^2\right]$, which depends on the LWA gain, therefore on (θ_d, ϕ_d). Fig. 6c and 6d show the angular distribution of the SNR used in numerical simulations with the LWACC and the LWASC, respectively. The SNR experienced by the (θ_1, ϕ_1) source is 13.1 dB with the LWACC and 12.1 dB with the LWASC while the SNR for the (θ_2, ϕ_2) source is 16.1 dB with the LWACC and 12.4 dB with the LWASC. As anticipated by the ρ behavior, the pseudospectrum cut along θ exhibits a single sharp peak, leading to accurate estimation of θ_1 with both antennas. Along ϕ, the LWACC does not show a clear peak at ϕ_1, and therefore fails to detect one of the two DoAs, owing to the high similarity of the response vectors in this angular range, as already expected from the flatness of ρ. The LWASC overcomes this issue thanks to its frequency-dependent radiation pattern along ϕ.

V. Conclusions

A novel fully metallic periodic LWA for passive 2D DoA estimation has been presented. The design employs a sectorial waveguide with corrugated metasurface on the bottom plate and periodic slots on the top plate. Two different corrugated metasurfaces were investigated, i.e. concentric and straight corrugations, resulting in an azimuth-independent (ϕ-isotropic) and azimuth-dependent (ϕ-anisotropic) directional pattern of the LWAs, respectively. The performance of the LWAs for 2D DoA estimation are evaluated using the MUSIC algorithm. An anisotropic design of the corrugations enables a correct DoA estimation of both elevation and azimuth angles with a single-port antenna. Future works will focus on breaking the symmetry of the pattern to avoid $\pm\hat{\phi}_d$ ambiguity and on experimental validations.

VI. Acknowledgements

This work was supported by the ANR BeSensiCom project, grant ANR22-CE25-0002 of the French Agence Nationale de la Recherche, Italian PRIN Grant 2017NT5W7Z GREEN TAGS, Next Generation EU within PNRR M4C2, Inv. 1.4-Avv. n.3138 6/12/2021-CN00000013 National Centre for HPC with resources provided by HPC@POLITO (http://hpc.polito.it)

References

[1] I. Uchendu, and J. Kelly, "Survey of Beam Steering Techniques Available for Millimeter Wave Applications," *Progress In Electromagnetics Research B*, vol. 68, pp. 35–54, 2016.

[2] S. Abilemona, H. V. Nguyen and C. Caloz, "Analog Direction of Arrival Estimation Using an Electronically-Scanned CRLH Leaky-Wave Antenna," *IEEE Transactions on Antennas and Propagation*, vol. 59, no. 4, pp. 1408–1412, 2011.

[3] D. Xia et al., "Accurate 2-D DoA Estimation Based on Active Metasurface With Nonuniformly Periodic Time Modulation," *IEEE Transactions Microwave Theory and Techniques*, vol. 71, no. 8, pp. 3424-3435, 2023.

[4] A. A. Oliner, "Leaky-wave antennas" in *Antenna Engineering Handbook*, J. L. Volakis, ch. 8, 4th ed., McGraw-Hill Education, 2007.

[5] D. B. Karmokar et al., "Continuous Backward-to-Forward Scanning 1-D Slot-Array Leaky-Wave Antenna With Improved Gain," *IEEE Antennas and Wireless Propagation Letters*, vol. 19, no. 1, pp. 89–93, 2020.

[6] M. Kuznetcov, D. Comite, S. K. Podilchak, P. Burghignoli, A. Galli, A. P. Freundorfer, Y M. M. Antar, and P. Baccarelli, "Half-Annular Leaky-Wave Antenna With Suppressed Open Stopband: Design and Experimental Testing," *IEEE Antennas and Wireless Propagation Letters*, vol. 22, no. 5, pp. 1204-1208, 2023.

[7] Z. Liu et al., "Partially Open Corrugated Waveguide Frequency Scanning Antennas With Linear and Circular Polarizations," *IEEE Transactions on Antennas and Propagation*, vol. 69, no. 10, pp. 6218-6228, 2021.

[8] H. -H. Zhang, J. Ren, W. Li, X. -Y. Sun, R. He, and Y. Yin, "Design of High-Scanning-Rate and Full-Space-Scanning Leaky Wave Antenna Utilizing the Manipulation of Slow Wave Dispersion Curve," *IEEE Transactions on Antennas and Propagation*, vol. 72, no. 9, pp. 7311-7316, 2024.

[9] M. Perrone, J. Sarrazin, G. Valerio and G. Lombardi, "Leaky-wave Analysis and Design of a Corrugated Sectoral Waveguide," in *International Conference on Electromagnetics in Advanced Applications (ICEAA)*, Lisbon, Portugal, pp. 662–666, 2024.

[10] J. Sarrazin and G. Valerio, "H-plane-scanning Multibeam Leaky-Wave Antenna for Wide-Angular-Range AoA Estimation at mm-Wave", *17th European Conference on Antennas and Propagation (EuCAP)*, Florence, Italy, pp. 1-4, 2023.

[11] A. Attar and A. R. Sebak, "High Gain Periodic 2-D Leaky-Wave Antenna With Backward Radiation for Millimeter-Wave Band," *IEEE Open Journal of Antennas and Propagation*, vol. 2, pp. 49–61, 2021.

[12] Z. Liu, H. Lu, J. Liu, S. Yang, Y. Liu and X. Lv, "Compact Fully Metallic Millimeter-Wave Waveguide-Fed Periodic Leaky-Wave Antenna Based on Corrugated Parallel-Plate Waveguides," *IEEE Antennas and Wireless Propagation Letters*, vol. 19, no. 5, pp. 806–810, 2020.

[13] D. Kampouridou, H. Lu, J. Liu, S. Yang, Y. Liu and X. Lv, "Full-Wave Leaky-Wave Analysis of 1-D Periodic Corrugated Metal Surface Antennas," *IEEE Antennas and Wireless Propagation Letters*, vol. 20, no. 5, pp. 863–867, 2021.

[14] T. Lira-Valdés, E. Rajo-Iglesias and F. Pizarro, "3-D-Printed Spiral Leaky Wave Antenna With Circular Polarization," *IEEE Open Journal of Antennas and Propagation*, vol. 4, pp. 427-433, 2023.

[15] R. Schmidt, "Multiple emitter location and signal parameter estimation," *IEEE Transactions on Antennas and Propagation*, vol. 34, no. 3, pp. 276-280, 1986.

[16] M. Poveda-García, E. Andreu-García, J. García-Fernández, D. C. Rebenaque and J. L. Gómez-Tornero, "Frequency-Scanned Leaky-Wave Antenna Topologies for Two-dimensional Direction of Arrival Estimation in IoT Wireless Networks," 2021 15th European Conference on Antennas and Propagation (EuCAP), Dusseldorf, Germany, 2021.

[17] F. E. Borgnis and C. H. Papas, "Electromagnetic Waveguides and Resonators" in *Electric Fields and Waves*, Springer, 1958.

[18] R. F. Harrington, "Cylindrical wave functions" in *Time-harmonic electromagnetic fields*, ch. 5, Wiley-IEEE Press, 2001.

[19] C. Balanis, "Rectangular cross-section waveguides and cavities" in *Advanced engineering electromagnetics*, ch. 8 and ch. 9, 2nd ed., Wiley, 2012.

[20] M. Bosiljevac, Z. Sipus and P.-S. Kildal "Construction of Green's functions of parallel plates with periodic texture with application to gap waveguides–a plane-wave spectraldomain approach," *IET Microw. Antennas Propag.*, vol. 4, no. 11, pp. 1799–1810, 2010.

[21] Z. Sipus, H. Merkel, and P.-S. Kildal "Green's functions for planar soft and hard surfaces derived by asymptotic boundary conditions," *IEE Proc. Microw. Antennas Propag.*, vol. 144, no. 10, pp. 321–328, 1997.

[22] R. Mittra and S. W. Lee, *Analytical Techniques in the Theory of Guided Waves*, New York, NY, USA: Macmillan, 1971

[23] A. Monorchio, R. Mittra, and G. Manara, "Generalized scattering matrix technique," in *Encyclopedia of RF and Microwave Engineering,* pp. 1767–1777, Ed. Hoboken, NJ, USA: Wiley, 2005.

[24] L. Wang, Y. Li, K. Ding, J. Wang, and B. Ai, "A Dual-Band Leaky Wave Antenna Fed by Dual-Mode-Composite Waveguide for Microwave and Millimeter-Wave Applications," *IEEE Transanctions on Antennas and Propagation*, vol. 72, no. 2, pp. 1965–1970, 2024.